Journal of Cluster Science (2021) 32:585–592
https://doi.org/10.1007/s10876-020-01816-5

ORIGINAL PAPER

# Facile Green Synthesis of Ag@g-$C_3N_4$ for Enhanced Photocatalytic and Catalytic Degradation of Organic Pollutant

Saran Sarangapany[1] · Kaustubha Mohanty[1,2]

Received: 22 February 2020 / Published online: 26 May 2020


## Abstract

A simple and easy green synthesis of silver nanoparticles (Ag NPs) was prepared using *Sapindus emarginatus* stem bark extract and anchored over graphitic carbon nitride (g-$C_3N_4$) surface. The synthesized materials characterized by UV–Visible, XRD, FESEM, FETEM, FT-IR and Raman spectroscopy ensured the development of Ag NPs anchored over the g-$C_3N_4$ surface. The prepared catalyst was utilized for Methylene Blue (MB) dye degradation through visible light photocatalysis. The optimization of operational parameters, like the effect of catalyst dosage, $H_2O_2$ concentration and slurry pH, was performed. The results exhibited that compared to pristine g-$C_3N_4$, photocatalytic efficacy was enhanced two-fold in Ag@g-$C_3N_4$. Also, the prepared Ag@g-$C_3N_4$ showed a faster catalytic MB dye reduction (25 s) in the presence of $NaBH_4$. The catalyst was recovered from the reaction solution by centrifugation and reused for five consecutive cycles. The results showed that there was no significant loss in the efficiency of the catalyst. These results confirmed that the green synthesized Ag@g-$C_3N_4$ is likely advantageous for organic pollutants degradation.

**Keywords** Green synthesis · Silver nanoparticles · Photocatalysis · Visible light · Organic pollutants

## Introduction

Presence of toxic organic compound in water is a severe threat to global human health. Photocatalytic mediated degradation of those harmful recalcitrant organic compound is becoming a promising treatment method [1]. Photocatalyst such as $TiO_2$, ZnO, CdS, WO and $C_3N_4$ have been employed for organic compounds degradation previously. Among them, graphitic carbon nitride (g-$C_3N_4$) mediated photocatalysis is gaining significant consideration because it has narrow bandgap, low cost, high stability and non-toxicity. However, due to its higher electron ($e^-$) and hole ($h^+$) recombination rate and lower utilization of visible light, limits it practical photocatalytic applications [2]. These limitations can be overcome by anchoring with noble metal nanoparticles such as Au, Pt, Pd and Ag, which traps the photogenerated electron and also enhances the visible light utilization [3]. Among these noble metals, silver is gaining much attention due to facile synthesis, tuning its size, shape and morphology, cost-effective when compared to other noble metals and activate the catalyst under visible region by its Localized Surface Plasmon Resonance (LSPR) property [4–6]. Synthesis of silver nanoparticles and anchoring over various semiconductor by chemical reduction, photo deposition, Wet impregnation, evaporation–condensation, laser ablation and biogenic method were demonstrated previously [7–11].

Biogenic mediated preparation of Ag NPs with the help of plant extracts has gained ample consideration than other methods because the phytochemicals act as reducing and stabilizing agents, easy availability and preparation, low cost and low toxic [12–15]. Recently, Kumar et al. [16] synthesized Ag@$TiO_2$ by using Rambutan peel extract and utilized it for enhanced photocatalytic degradation of MB dye. Likewise, Tahir et al. 2016 [17] developed Ag/$TiO_2$ using *Cestrum nocturnum* leaf extract and used it for enhanced photocatalytic MB Dye. Sohrabnezhad and Seifi

**Electronic supplementary material** The online version of this article (https://doi.org/10.1007/s10876-020-01816-5) contains supplementary material, which is available to authorized users.

✉ Kaustubha Mohanty
kmohanty@iitg.ac.in

[1] Centre for the Environment, Indian Institute of Technology Guwahati, Guwahati 781039, India

[2] Department of Chemical Engineering, Indian Institute of Technology Guwahati, Guwahati 781039, India

[18] utilized *Urtica dioica* leaf extract for the synthesis of Ag/ZnO to improve its photocatalytic activity towards MB dye degradation under visible light. Similarly, Sorbiun et al. 2018 [19] green synthesized Ag/ZnO using oak fruit hull to increase its photocatalytic activity towards basic violet 3 dye degradation. The green synthesis of Ag@g-$C_3N_4$ using plant extract and its application on photocatalytic degradation was limited [20, 21]. Hence the present study was aimed to utilize the phytochemicals present in the *Sapindus emarginatus* stem bark for the preparation of Ag NPs, and it was anchored over the g-$C_3N_4$ surface. The prepared particles were utilized for enhanced photocatalytic and catalytic degradation of MB dye.

## Materials and Methods

### Materials

Analytical grade (AR) Melamine, silver nitrate, sodium hydroxide, sulphuric acid, methylene blue, sodium borohydride, and hydrogen peroxide were purchased from Merck India Ltd and utilized. Double distilled water was used for reagent preparation and experiment purposes.

### Preparation of Bark Extract

*Sapindus emarginatus* stem bark was collected from IIT Guwahati campus and shade dried for 1 week. The bark was grounded into a fine powder using a mechanical grinder. For the preparation of aqueous bark extract, stem bark powder of about 10 g was added with 100 ml of double-distilled water and refluxed at 65 °C for half an hour. The sample was cooled, filtered and preserved at 4 °C for further purpose.

### Preparation of Pristine g-$C_3N_4$

By simple polymerization of melamine, g-$C_3N_4$ was prepared by heating in a muffle furnace for 2 h at 550 °C with a ramp increment of 5 °C $min^{-1}$ under Nitrogen condition. The obtained yellow powder was ground well and exfoliated by the ultra-sonication process [22].

### Green Synthesis of Ag@g-$C_3N_4$

*Sapindus emarginatus* bark extract was utilized for the formation of Ag NPs anchored over g-$C_3N_4$. In a typical procedure, 500 mg of g-$C_3N_4$ was added with 50 ml of $AgNO_3$ solution (100 ppm Ag) and sonicated for 30 min for the dispersion of particles. The above solution was mixed with 10 ml of bark extract as a reducing agent, and the solution was stirred at 500 rpm for 2 h for the formation of Ag NPs. The resultant solution was dried at 120 °C in a hot air oven for 48 h and sintered at 450 °C for 2 h. The powder was cooled and grounded well and stored for further usage.

### Characterization Studies

The preliminary confirmation of silver NPs formation was measured by using UV–Visible spectrophotometer (Shimadzu UV 1900). The diffused reflectance spectra of pristine and Ag anchored g-$C_3N_4$ was measured using UV-Vis. NIR. Spectrophotometer (Varian, 5000). The crystalline structure and phase of the prepared particles were measured using powder X-ray diffractometer (Rigaku, SmartLab). The surface morphology, size and shape of NPs were measured using FESEM (Zeiss, Sigma 300), and high-resolution TEM image was obtained using FETEM (JEOL, 2100F). The elemental mapping of Ag@g-$C_3N_4$ was analyzed using EDX (Thermofisher) attached in the FESEM. The functional group present in the plant extract and prepared particles were analyzed using FTIR (PerkinElmer, Spectrum Two). The Raman scattering of prepared samples was measured using Raman Spectrophotometer (Horiba, LABRAMAN). The photoluminescence spectra were obtained using a spectrofluorometer (JY Fluorolog—FL3-11) by exciting the sample at 360 nm.

### Photocatalytic Activity

The prepared particles were tested for Methylene blue (MB) dye degradation. For photocatalytic studies, 100 ml of MB solution (10 ppm) was taken in 250 ml beaker and mixed with 50 mg of prepared particles and sonicated for 30 min for dispersion of particles. The samples were then exposed under 350 W Xenon lamp with 420 nm cutoff filter with constant stirring. The samples were withdrawn at constant intervals, and the catalyst was removed by centrifugation. The resultant supernatant was examined by spectrometry to estimate the degradation percentage of MB dye.

### Catalytic Dehydrogenation

The catalytic efficacy of the synthesized particles was assessed by MB dye dehydrogenation reaction with the existence of $NaBH_4$. The catalytic reaction was performed in a 3 cm cuvette by mixing 2 ml of MB dye (50 ppm) along with 1 ml of $NaBH_4$ solution (0.1 M). To initiate the catalytic reaction, 2.0 mg of the Ag@ g-$C_3N_4$ was added and mixed well. The absorbance was recorded with UV–Vis. Spectrophotometer, after removing the catalyst from the solution by centrifugation.

### Reuse and Recyclability Test

The reuse and recyclability test was performed up to five successive cycles by recovering the catalyst from the solution by centrifugation, washed and dried at 90 °C in a hot air oven.

## Results

### Characterization Results

The development of Ag NPs with the help of bark extract of *Sapindus emarginatus* was examined preliminary by using UV–Vis. Spectroscopy. Figure 1a ensures the development of Ag NPs by exhibiting a strong absorption peak at 450 nm ascribed to surface Plasmon resonance (SPR) properties of Ag NPs [23, 24]. The optical properties of pristine g-$C_3N_4$ and Ag@ g-$C_3N_4$ was measured by diffused reflectance spectra (Fig. 1b). Pristine g-$C_3N_4$ showed absorption edge at 460 nm ascribed to 2.7 eV of optical bandgap energy.

In contrast, the Ag@g-$C_3N_4$ exhibited extended wavelength with redshift in the visible region due to the SPR effect of nano-sized Ag anchored over the surface of g-$C_3N_4$. The UV- Vis. Spectra confirm that Ag@g-$C_3N_4$ can utilize visible light better than pristine [25].

Figure 2 illustrated the crystalline nature of pure g-$C_3N_4$ and green synthesized Ag@g-$C_3N_4$ were analyzed using PXRD. From the result, it was clear that both the samples exhibited hexagonal phase of g-$C_3N_4$ with a significant peak at 27° allotted to (002) plane of aromatic interlayer stacking segments and another minor peak at 13°

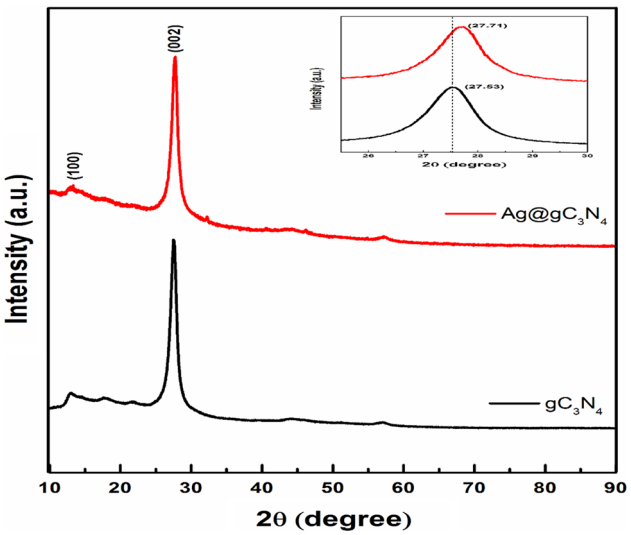


**Fig. 2** PXRD spectra of pristine g-$C_3N_4$ and Ag@g-$C_3N_4$

consigned to crystal (100) plane of tris-s-triazine. Compared to pristine, Ag@g-$C_3N_4$ (Fig. 2 inset) showed a shift from 27.53° to 27.72°, which denoted a decrease in the gallery distance between pristine g-$C_3N_4$, and Ag@g-$C_3N_4$. There were no diffraction peaks of Ag observed due to lower loading percentage (1wt %) and well dispersion of Ag NPs in the Ag@g-$C_3N_4$ [26].

The structural, shape and morphological characteristic of pristine and Ag@g-$C_3N_4$ were obtained using FESEM and FETEM analysis. The morphology of pristine g-$C_3N_4$ and Ag@g-$C_3N_4$ was measured by FESEM (Fig. S1) reveals that both the samples are irregular in shape with strong agglomeration with other particles. There were not many morphological modifications observed between the

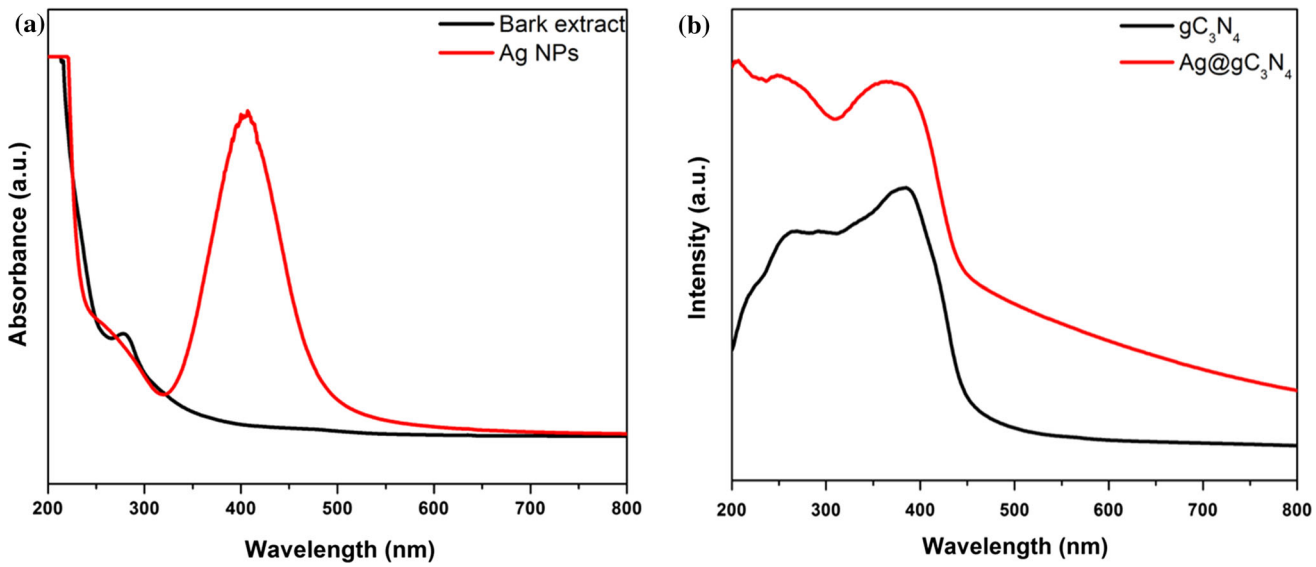


**Fig. 1** UV-Visible absorption spectra of **a** plant extract and Ag Nps and **b** DRS spectra of pristine g-$C_3N_4$ and Ag@g-$C_3N_4$

pristine and Ag@g-$C_3N_4$ particles. Whereas, the FETEM image of Ag@g-$C_3N_4$ (Fig. 3) displayed the existence of spherical Ag NPs with an average size of 16 nm, which was uniformly anchored over the g-$C_3N_4$ surface. The TEM image (Fig. S2) of pristine g-$C_3N_4$ confirmed that the sheet-like structure was formed. The elemental mapping of Ag@g-$C_3N_4$ was illustrated in Fig. 4 ensures the existence of silver beside with nitrogen, carbon and a small percentage of oxygen. The TEM image and EDX mapping clearly display that Ag NPs was distributed uniformly on the g-$C_3N_4$ surface.

The FTIR spectra of bark extract, pristine g-$C_3N_4$ and Ag@g-$C_3N_4$ are illustrated in Fig S3. The FTIR spectra of bark extract exhibit peak at 3330 $cm^{-1}$ and 2903 $cm^{-1}$ corresponds to O–H bond stretching of the phenolic group and C-H stretching of alkene bond respectively. The intense peak at 1606 $cm^{-1}$ and 1033 $cm^{-1}$ were ascribed to N=H and C–O of secondary amide and ether groups, respectively [27, 28]. The FTIR peak of both pristine and Ag anchored g-$C_3N_4$ with similar peaks confirmed that anchoring of Ag NPs did not alter the g-$C_3N_4$ original structure. The FTIR spectrum of g$C_3N_4$ showed a broad peak at 3000 $cm^{-1}$ to 3300 $cm^{-1}$ related to stretching vibration of the N–H group. In contrast, many peaks situated in the range of 1200 $cm^{-1}$ to 1650 $cm^{-1}$ corresponded to CN heterocycles, while the sharp peak at 808 $cm^{-1}$ ascribed to s-triazine breathing mode [29]. From the FTIR spectrum, it was clear that phytochemicals such as polyphenols, flavonoids and other organic compounds play a pivotal role in the synthesis of Ag NPs, which acts as reducing, stabilizing and capping agents.

Raman spectra of g-$C_3N_4$ and Ag@g-$C_3N_4$ (Fig. S4) illustrated that pristine g-$C_3N_4$ did not display a significant Raman signal, whereas the Ag NPs anchored g-$C_3N_4$ showed a surface-enhanced Raman scattering spectrum. The strong Raman spectral band seen at 1570 $cm^{-1}$ matches with vibrational stretching of C-N bond and peak at 550 $cm^{-1}$ relates to heptazine heterocyclic vibrational stretch. The peak at 1240 $cm^{-1}$ denoted the CN heterocyclic vibrational mode. The intensity of Raman spectra was significantly enhanced in Ag@g-$C_3N_4$ due to the transferring of charge between Ag and g-$C_3N_4$ molecule [26]. This result ensures that there is a strong interface existed with g-$C_3N_4$ and Ag NPs, which facilitate the charge transfer between them.

The photoluminescence (PL) spectra of pristine and Ag@g-$C_3N_4$ was measured with an excitation at 360 nm to study the transfer, migration and photogenerated $e^-$ and $h^+$ recombination rate. From Fig. 5, it was clear that the PL intensity of Ag@g-$C_3N_4$ was quenched notably than pristine g-$C_3N_4$. The results suggested that Ag NPs acted as an electron trap thereby it decreased the $e^-$ and $h^+$ recombination process leads to increased the formation of more radicles leads to boosted photocatalytic efficiency of Ag@g-$C_3N_4$ [30].

## Photocatalytic Degradation of MB Dye

The photocatalytic efficacy of the prepared Ag@g-$C_3N_4$ was assessed towards MB dye degradation. The experiments were executed with pristine, Ag@g-$C_3N_4$, and by photolysis was shown in Fig. 6. The results reveal that pristine g-$C_3N_4$ has less efficacy (42%) to degrade MB dye, due to fast electron–hole recombination rate. Whereas, Ag@g-$C_3N_4$ showed a nearly two-fold increase in photocatalytic MB dye (99%) degradation exposed under visible light for 1 h. The adsorption capacity of the catalyst was performed under the dark condition. The results showed that nearly 14% of dye was adsorbed over the catalyst surface after 2 h contact between dye and the catalyst. The increased photocatalytic activity of Ag@g-$C_3N_4$ was due to electron trapping ability of Ag NPs, in turn, reduces

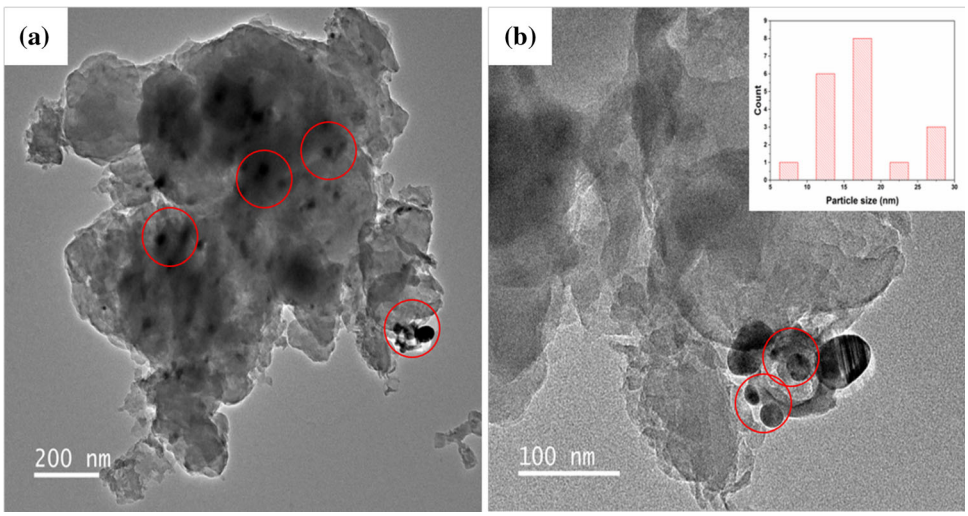


**Fig. 3** FE-TEM image of Ag@g-$C_3N_4$ (Red circle showing Ag NPs) and inset showing particle size histogram of Ag NPs (Color figure online)

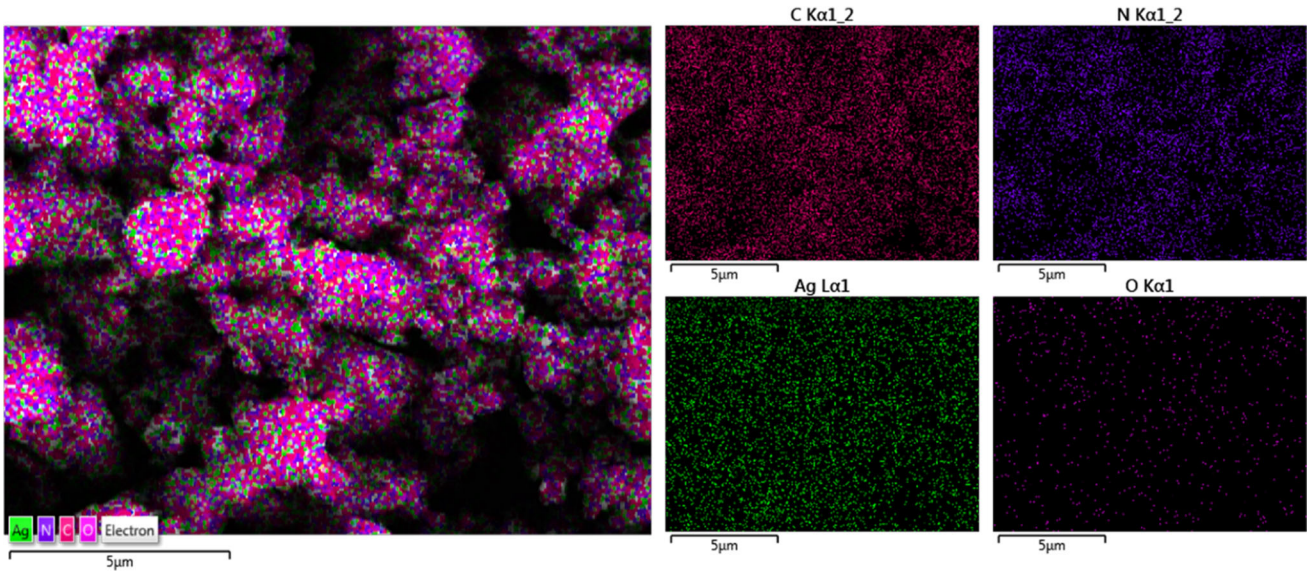


**Fig. 4** EDX mapping of Ag@g-$C_3N_4$

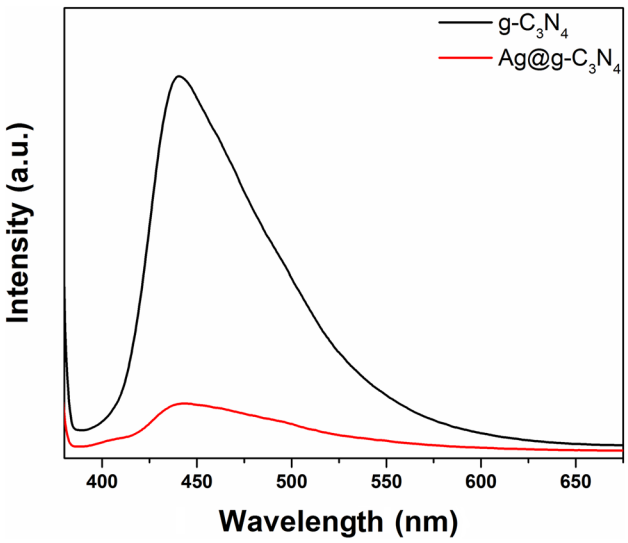


**Fig. 5** Photoluminescence spectra of pristine g-$C_3N_4$ and Ag@g-$C_3N_4$

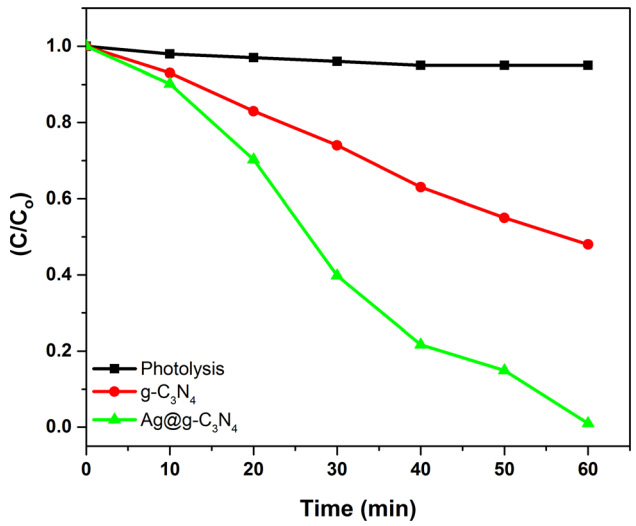


**Fig. 6** Photocatalytic degradation MB dye by photolysis, pristine g-$C_3N_4$ and Ag@g-$C_3N_4$ under visible light irradiation (Catalyst Conc: 50 mg/l, Dye Conc.: 10 ppm, Time: 60 min, pH:7)

electron and hole rejoining rate, which increases the formation of ROS [31]. Only negligible degradation of MB dye observed when the dye was exposed under direct light without any catalyst. Ag@g-$C_3N_4$ has been selected to optimize the reaction parameters since it showed higher degradation towards MB dye.

## Effect of Catalyst Concentration

To optimize the catalyst dosage on MB dye degradation, the experiment was performed with different catalyst concentration from 100 ppm to 1000 ppm. Figure 7 depicts the influence of the different catalyst dosages on the percentage degradation of MB dye after 60 min exposed under 350 W Xenon lamp. The results reveal that a gradual increment in the efficiency of the MB dye degradation was observed from 100 ppm to 500 ppm, and additional increment in the catalyst dosage led to a reduction in the degradation rate. The initial increment in dye degradation because of increment in the active surface with increasing catalyst dosage. Whereas, a decrease in the degradation rate with further increment in catalyst concentration was observed due to the screening effect of suspended particles which hampers the light penetration [32].

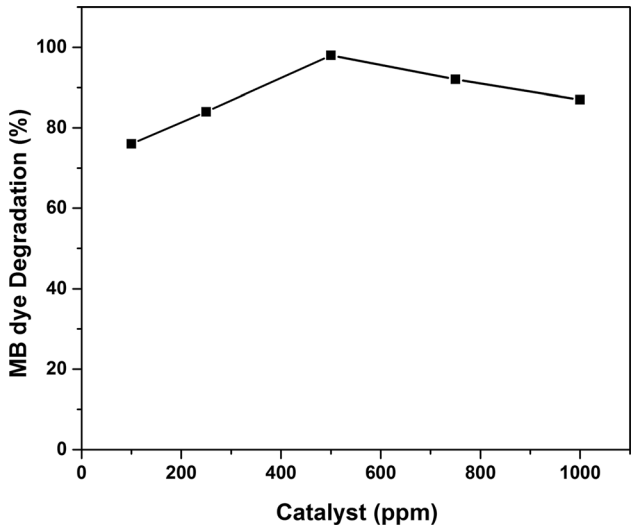


**Fig. 7** Effect of various catalyst concentration on photocatalytic degradation MB using Ag@g-$C_3N_4$ (Dye Conc.: 10 ppm, Time: 60 min, pH:7)

## Effect of Initial Slurry pH

To study the effect of initial slurry pH on dye degradation, the testing was performed with different pH from 2 to 10 (Fig. 8). The results illustrated that there was a gradual increment in the MB dye degradation seen when the pH of the slurry was adjusted from acidic to alkaline. Under the alkaline condition, the catalyst surface becomes more positively charged, which attracts more dye molecules towards it and thereby increasing the rate of degradation under alkaline compared to the acidic condition [33].

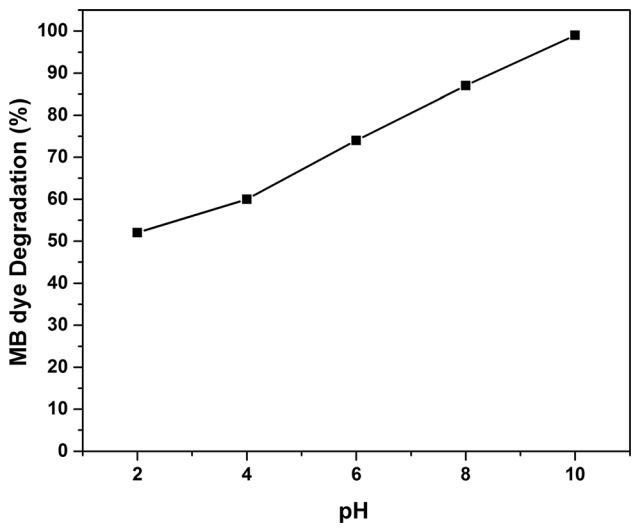


**Fig. 8** Effect of pH on photocatalytic degradation MB using Ag@g-$C_3N_4$ (Catalyst Conc: 50 mg/l, Dye conc.: 10 ppm, Time: 45 min)

## Effect of $H_2O_2$ Concentration

The effect of the oxidizing agent on MB dye degradation was conducted with various concentration of $H_2O_2$ ranging from 0 mM to 5 mM. Figure 9 infers that the amount of dye degradation was improved with increasing the peroxide dosage because $H_2O_2$ was acting as electron scavenger thereby sinking the $e^-$ and $h^+$ recombination rate which increases the formation of more radicals in the reaction system. Also, $H_2O_2$ may dissociate photocatalytic into $^oOH$ radicals, thus enhancing the photocatalytic efficiency [34].

## Possible Mechanism Of Photocatalytic Degradation of MB Dye

The possible mechanism behind the photocatalytic MB dye degradation using Ag@g-$C_3N_4$ was illustrated in Fig. 10. When the sample was irradiated with visible light, it activates the charge separation process, which leads to the development of condition band $e^-$ and $h^+$ in the valance band. The Ag NPs anchored over the g-$C_3N_4$ traps the conduction band electron decrease the $e^-$ and $h^+$ recombination rate resulted in enhanced photocatalytic degradation which was observed with Ag@ g-$C_3N_4$ comparted to pristine. The electron trapped by the Ag NPs reduces the molecular $O_2$ into $O_2^-$superoxide radical anion, and $h^+$ can react directly with dye solution or split the water into °OH radicals. These photogenerated radicals and $h^+$ plays a vital role in the degradation of MB dye [35].

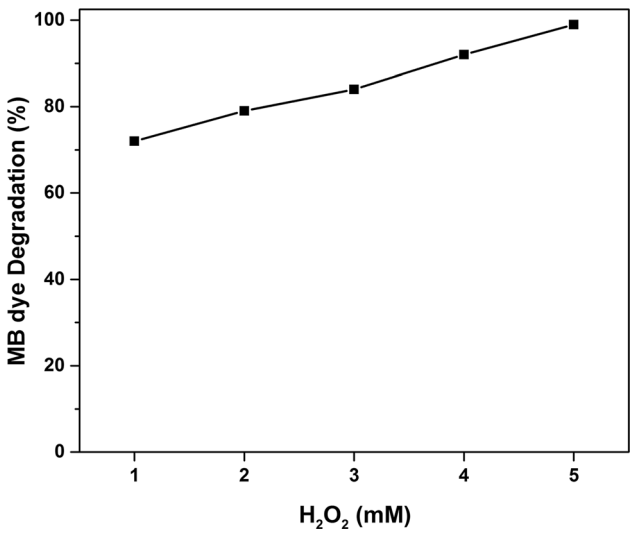


**Fig. 9** Effect of $H_2O_2$ concentration on photocatalytic degradation MB using Ag@g-$C_3N_4$ (Catalyst Conc: 50 mg/l, Dye Conc.:10 ppm, Time: 30 min, pH: 7)

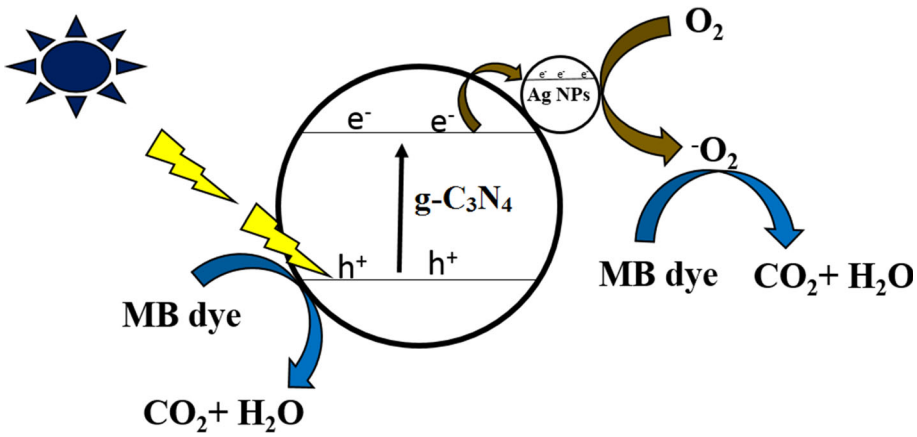


**Fig. 10** Possible Mechanism of photocatalytic degradation MB dye using Ag@g-$C_3N_4$ under visible light

## Catalytic Reduction of MB Dye

The catalytic ability of Ag@g-$C_3N_4$ was evaluated for the reduction of MB dye with the existence of $NaBH_4$. Figure 11 shows the fast reduction of MB to Leuco methylene blue (LMB), which was observed within 25 s confirmed by decreased in the intensity of adsorption peak at 664 nm. No reduction in the adsorption peak of MB dye was observed when the reaction is conducted with pristine g-$C_3N_4$ [36, 37].

## Recovery and Reuse of the Catalyst

The catalyst was recovered by centrifuging the sample at 6000 rpm, and the recovered catalyst was reused up to 5 successive cycles to check its photocatalytic and catalytic efficiencies (Fig. 12). The results exhibited that the Ag@ g-$C_3N_4$ showed improved photocatalytic degradation (∼ 84%) and catalytic reduction of MB (∼ 94%) after five cycles which confirmed that the prepared particles were effective and stable for the reduction and degradation of MB dye. The stability of the Ag@ g-$C_3N_4$ catalyst after the 5$^{th}$ cycle was verified using TEM (Fig. S5) and XRD (Fig. S6) analysis. The results revealed that there is no morphological, and crystalline changes observed even after five cycles, which ensured that the catalyst is more stable and can be reused several times.

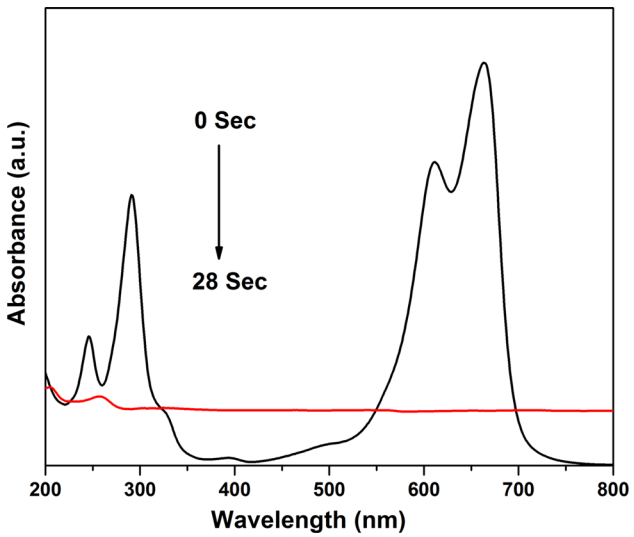


**Fig. 11** Catalytic reduction of MB dye by Ag@g-$C_3N_4$ in the presence of $NaBH_4$

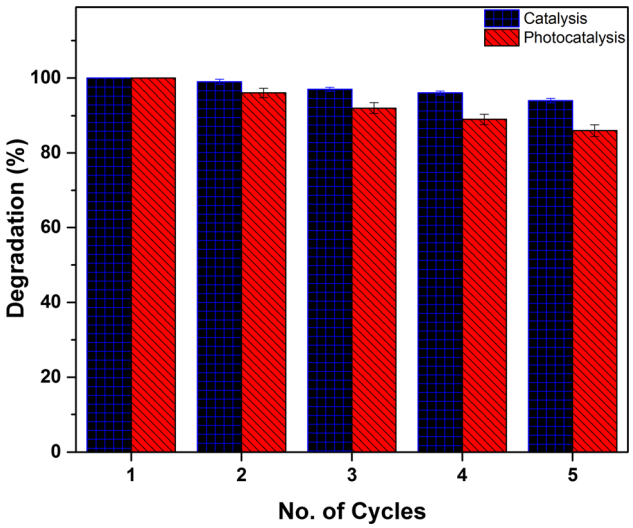


**Fig. 12** Reuse and recyclability of the Ag@g-$C_3N_4$ towards photocatalytic and catalytic degradation of MB dye

## Conclusion

A facile and simple biogenic mediated Ag NPs was prepared and anchored over g-$C_3N_4$ using the aqueous stem bark extract of *Sapindus emarginatus*. The phytochemicals compound in the bark extracts act as reducing and stabilizing agent for Ag NPs synthesis. The characterization results ensured the anchoring of Ag NPs over the g-$C_3N_4$ surface. The synthesized catalyst was utilized for the

visible light active catalyst for MB dye degradation. Compared to pristine, Ag@ g-$C_3N_4$ showed better photocatalytic activity under visible region and good catalytic reduction of MB dye. Addition of oxidizing agent ($H_2O_2$) and alkaline slurry pH enhance the rate of photocatalytic degradation. The prepared Ag@g-$C_3N_4$ catalyst also showed excellent stability and recyclability even after 5 successive cycles. This study provided an easy, and greener method for the preparation of Ag anchored g-$C_3N_4$ for efficient organic pollutants degradation.

**Acknowledgement** The authors acknowledge Central Instrumental Facility (CIF), Department of Chemical Engineering and Center for the Environment, Indian Institute of Technology Guwahati for characterization studies. The first author is thankful to IIT Guwahati for providing Institutional Post-Doctoral fellowship.

## Compliance with Ethical Standards

**Conflict of interest** The authors declare that they have no conflict of interest.

## References

1. N. Cheng, J. Tian, Q. Liu, C. Ge, A. H. Qusti, A. M. Asiri, A. O. Al-Youbi, and X. Sun (2013). *ACS Appl. Mater. Inter.* **5**, 6815.
2. X. Han, L. An, Y. Li, C. Hou, H. Wang, and Q. Zhang (2020). *Appl. Cat. B: Environ.* **265**, 118539.
3. A. Mohammad, M. R. Karim, M. E. Khan, M. M. Khan, and M. H. Cho (2019). *J. Phys. Chem. C* **123**, 20936.
4. A. Hatamifard, M. Nasrollahzadeh, and S. M. Sajadi (2016). *New J. Chem.* **40**, 2501.
5. S. Saran, P. Arunkumar, G. Manjari, and S. P. Devipriya (2019). *Environ. Technol.* **40**, 3190.
6. M. Maryami, M. Nasrollahzadeh, E. Mehdipour, and S. M. Sajadi (2016). *Int. J. Hydrog. Energy* **41**, 21236.
7. S. Saran, P. G. Kamalraj, G. Arunkumar, and S. P. Devipriya (2016). *Environ. Sci. Pollut. Res.* **23**, 17730.
8. L. Tang, C. Feng, Y. Deng, G. Zeng, J. Wang, Y. Liu, H. Feng, and J. Wang (2018). *Appl. Cat. B: Environ.* **230**, 102.
9. C. H. Liu, M. H. Hong, Y. Zhou, G. X. Chen, M. M. Saw, and A. T. S. Hor (2007). *Physica Scripta* **T129**, 326.
10. L. G. Devi and R. Kavitha (2016). *Appl. Surf. Sci.* **360**, 601.
11. G. Manjari, S. Saran, S. P. Devipriya, and A. V. B. Rao (2018). *Catal. Lett.* **148**, 2561.
12. G. Manjari, S. Saran, T. Arun, S. P. Devipriya, and A. V. B. Rao (2017). *J. Clust. Sci.* **28**, 2041.
13. M. Nasrollahzadeh, S. Mahmoudi-Gom Yek, N. Motahharifar, and M. Ghafori Gorab (2019). *Chem. Rec.* **19**, 2436.
14. M. Sajjadi, M. Nasrollahzadeh, and S. M. Sajadi (2017). *J. Colloid Interface Sci.* **497**, 1.
15. B. Khodadadi, M. Bordbar, and M. Nasrollahzadeh (2017). *J. Colloid Interface Sci.* **493**, 85.
16. B. Kumar, K. Smita, Y. Angulo, and L. Cumbal (2016). *Green Process. Synth.* **5**, 371.
17. K. Tahir, A. Ahmad, B. Li, S. Nazir, A. U. Khan, T. Nasir, Z. U. H. Khan, R. Naz, and M. Raza (2016). *J. Photochem. Photobiol. b. Biol.* **162**, 189.
18. S. Sohrabnezhad and A. Seifi (2016). *Appl. Surf. Sci.* **386**, 33.
19. M. Sorbiun, E. S. Mehr, A. Ramazani, and S. T. Fardood (2018). *Mater. Electron.* **29**, 2806.
20. K. Tian, W. J. Liu, and H. Jiang (2015). *ACS Sustain. Chem. Eng.* **3**, 269.
21. P. C. Nagajyothi, M. Pandurangan, S. V. P. Vattikuti, C. O. Tettey, T. V. M. Sreekanth, and J. Shim (2017). *Sep. Purif. Technol.* **188**, 228.
22. S. Tonda, S. Kumar, M. Bhardwaj, P. Yadav, and S. Ogale (2018). *ACS Appl. Mater. Inter.* **10**, 2667.
23. Y. K. Mohanta, S. K. Panda, R. Jayabalan, N. Sharma, A. K. Bastia, and T. K. Mohanta (2017). *Front. Mol. Biosci.* **4**, 14.
24. G. Manjari, A. Parthiban, and S. Saran (2019). *J. Clust. Sci.*. https://doi.org/10.1007/s10876-019-01721-6.
25. K. Qi, Y. Li, Y. Xie, S. Y. Liu, K. Zheng, Z. Chen, and R. Wang (2019). *Front. Chem.* **7**, 91.
26. H. Li, Y. Jing, X. Ma, T. Liu, L. Yang, B. Liu, S. Yin, Y. Wei, and Y. Wang (2017). *RSC Adv.* **7**, 8688.
27. N. Mir, M. Bahrami, E. Safari, and S. M. Hosseinpour-Mashkani (2015). *J. Clust. Sci.* **26**, 1113.
28. B. Khodadadi, M. Bordbar, and M. Nasrollahzadeh (2017). *J. Colloid Interface Sci.* **490**, 1.
29. M. Induja, K. Sivaprakash, and S. Karthikeyan (2019). *Mater. Res. Bull.* **112**, 331.
30. Y. Sun, T. Xiong, Z. Ni, J. Liu, F. Dong, W. Zhang, and W. K. Ho (2015). *Appl. Surf. Sci.* **358**, 356.
31. L. Ge, C. Han, J. Liu, and Y. Li (2011). *Appl. Cat. A: Gen.* **409**, 215.
32. M. S. Dorraji, A. R. Amani-Ghadim, M. H. Rasoulifard, H. Daneshvar, B. S. Z. Aghdam, A. R. Tarighati, and S. F. Hosseini (2017). *Chem. Eng. Res. Des.* **127**, 113.
33. P. Murugesan, N. Girichandran, S. Narayanan, and M. Manickam (2018). *Opt. Mater.* **75**, 431.
34. A. Kumar, A. Kumar, G. Sharma, H. Ala'a, M. Naushad, A. A. Ghfar, C. Guo, and F. J. Stadler (2018). *Chem. Eng. J.* **339**, 393.
35. M. E. Khan, T. H. Han, M. M. Khan, M. R. Karim, and M. H. Cho (2018). *ACS Appl. Nano Mater.* **1**, 2912.
36. Y. Fu, T. Huang, L. Zhang, J. Zhu, and X. Wang (2015). *Nanoscale* **7**, 13723.
37. M. Nasrollahzadeh, M. Bagherzadeh, and H. Karimi (2016). *J. Colloid Interface Sci.* **465**, 271.